Case Studies in Construction Materials 17 (2022) e01324

Contents lists available at ScienceDirect

Case Studies in Construction Materials

journal homepage: www.elsevier.com/locate/cscm

Experimental and simulation study on the impact resistance of concrete to replace high amounts of fine aggregate with plastic waste

Mustafa Maher Al-Tayeb [a], Yazan I. Abu Aisheh [b], Shaker M.A. Qaidi [c], Bassam A. Tayeh [d,*]

[a] School College of Applied Engineering and Urban Planning, University of Palestine, PO Box 1075, Gaza, Palestine
[b] Department of Civil Engineering, Middle East University, Amman 11831, Jordan
[c] Department of Civil Engineering, College of Engineering, University of Duhok, Duhok, Kurdistan Region, Iraq
[d] Civil Engineering Department, Faculty of Engineering, Islamic University of Gaza, P.O. Box 108, Gaza Strip, Palestine

ARTICLE INFO

Keywords:
Compressive strength
Impact resistance
Flexural resistance
Plastic concrete
Recycling
Sustainability

ABSTRACT

The impact of substantial amounts of plastic waste (PW) substituted fine aggregate (FA) on the mechanical characteristics of concrete under impact load (I.L) was studied experimentally-and-numerically. As fine aggregate substitutes, samples were made with 0%, 20%, 30%, and 40% PW. Six prisms of 100 mm width, 50 mm depth, and 400 mm length were loaded to failure in a drop-weight impact machine after 28 days by exposing them to 30 N of weight from a 400 mm height, while another three prisms of the same size and age were evaluated under static load(S.L). The load-displacement(L-D) and fracture energy(G_F) of normal and concrete with PW prisms under S.L and I.L were investigated. A 3D finite element technique simulation was also carried out using LUSAS V.14 to investigate the impact of L-D behavior, and the predictions were confirmed by experimental findings. Despite reducing the fine aggregate amount, it was discovered that a proportionate increase of PW up to 20% can lead to improvements in bending load, impact tup, and inertial load.

1. Introduction

Because of the health risks and difficulties in the land filling, the disposal of PW is a severe environmental concern all over the world [1]. The expensive expense of disposal, combined with the need for a vast landfill area, often leads to the indiscriminate and illegal dumping of PW {M. Al-Tayeb, 2021 #14}. As a result, there is an urgent need to develop alternate ways of reusing the PW for other purposes, and concrete has been recognized as one of the viable choices [2,3]. This is consistent with core ecological measures for instance waste avoidance, waste recycling, avoiding landfills, recovering energy from waste, and conserving raw resources [4]. Concrete, on the other side, has restricted characteristics; for example, poor tensile strength, impact energy absorption, and ductility [5,6]. Many concrete components and constructions are susceptible to I.Ls, such as bridge decks, wall panels, industrial floors, and hydraulic systems, as well as highway paving and airport pavements. Consequently, greater impact resistance (IR) and load-bearing capability are needed in these applications [7,8]. In this context, [9–12] demonstrated that fiber-reinforced materials have the capacity

* Corresponding author.
E-mail address: btayeh@iugaza.edu.ps (B.A. Tayeh).

https://doi.org/10.1016/j.cscm.2022.e01324
Received 20 April 2022; Received in revised form 25 June 2022; Accepted 16 July 2022
Available online 19 July 2022

to solve concrete brittleness. The use of metal waste fibers in the manufacturing of concrete has shown a solution for sustainable and green building, with the added bonus of a safe option for PW disposal [11]. Mohammadhosseini, Tahir and Sam [11] investigated reinforced concrete using waste metalized PW fibers in their research. They found that adding these waste fibers could have a big effect on the strength and IR development of concrete composites.

Several forms of PW have been studied in recent years, including high-density polyethylene (HDPE), polyethylene terephthalate (PET), and polypropylene (PP). This research focused on the impact of adding PW on the workability of fresh mixes and the strength of hardened mixes [13].

Ismail and Al-Hashmi [14] discovered that as the amount of PW (80%polyethylene and 20%polystyrene) rises, so does the bulk density and the workability. This is owing to the reduced density of PW aggregate in comparison to traditional aggregate. Naik, Singh, Huber and Brodersen [15] discovered that post-consumer waste high-density polyethylene plastic may be utilized impact live as a soft filler in concrete. They discovered that chemical treatment had a substantial impact on the behavior of the PW filler in concrete. According to [16], concrete incorporating PW particles from vehicle bumpers is more ductile than comparable forms of concrete prepared with traditional aggregate. This ductile behavior might be very beneficial in reducing fracture development in concrete construction. Furthermore, as the number of PW particles grew, the compressive and splitting tensile strengths of the concrete dropped.

The impact of high amounts of fine aggregate substitution by 20%, 30%, and 40% PW on the L-D and G_F of prisms subjected to I.L was investigated experimentally in this study, and the findings were compared with those obtained under S.L and by FEM simulations by means of the Lucas software. In this study, the author states the following contributions:

1. Investigation of I.L and consequent displacement and G_F in concrete with large PW amounts.
2. FEM-based numerical simulation of the L-D behavior of concrete containing PW particles; no previous simulation work on concrete PW particles has been described.

2. Materials and methods

2.1. Materials

Ordinary Portland cement (OPC) (ASTM Type I) was utilized in this investigation. Table 1 shows the chemical components of OPC.

As for the controlled mix, concrete with a CS of 45 MPa was produced. The largest coarse aggregate size was 10 mm, and the coarse aggregate specific gravity was 2.64. At room temperature and moisture, the bulk density and specific gravity of normal silica fine aggregate are 1730 kg/m3 and 2.65, respectively. In this investigation, polycarbonate particles derived from industrial waste were employed. Table 2 shows the particle size distribution of PW aggregate. Photographs of PW aggregate are illustrations in Fig. 1. Table 3 presents their physical and mechanical characteristics.

Concrete mixes were created with fine aggregate amount substitutions of 20%, 30%, and 40% (PW 20%, PW 30%, and PW 40%) with PW of particle size 3–4 mm. Table 4 shows the compositions of concrete with PW. Fig. 1 depicts the PW picture utilized in the current investigation.

Three cylinders of 200 mm height and 100 mm diameter were utilized for each kind of compression and elastic modulus (MOE) test. Six prisms of each kind of combination were constructed for the three-point impact flexural loading test. The testing prisms measured 50 mm in depth, 100 mm in width, and 400 mm in length, with a loaded span of 300 mm. All PW specimens pass the minimum requirement by the standard. For each example, three prisms of the same size were produced for the three-point static flexural loading test. In line with ASTM C-192/C-192M [17], all samples were cured in water for 28-d.

Table 1
Cement chemical compositions.

Minerals composition	
C_3S	63.12
C_2S	9.60
C_3A	8.19
C_4AF	9.95
Item	Percentage in Cement (%)
SiO_2	19.96
Fe_2O_3	3.28
Al_2O_3	5.18
MgO	0.78
SO_3	2.39
CaO	64.18
Total alkalies	0.92
Insoluble Residue	0.22
Loss on Ignition	2.51

Table 2
Fine aggregate and PC plastic aggregate particle size distribution.

Sieve size (mm)	Cumulative passing (%)	
	PW	Fine aggregate
4.75	100	100
3.15	25	77
2.36	4.5	43
1.18	0.95	18
0.6	0	7
0.3	0	1

Fig. 1. PW sample.

Table 3
Mechanical and physical characteristics of PW aggregate.

Characteristics	PWs
Unit weight (kg/m^3)	655
SG	1.22
Color	Black
Elastic Modulus (MPa)	2610

Table 4
PW concrete mixture characteristics.

Unit	PW %	Cement	Coarse aggregate	Fine aggregate	Water	PW
Wight(kg)	–	·400	970	·800	200	0
Amount(m^3)	0%	127	368	305	200	0
Wight (kg)	–	400	970	644	200	73
Amount(m^3)	20%	127	368	244	200	61
Wight (kg)	–	400	970	560	200	110
Amount(m^3)	30%	127	368	214	200	92
Wight (kg)	–	400	970	480	200	146
Amount(m^3)	40%	127	368	183	200	61

2.2. Experimental setup and procedure

ASTM C-469 [18] and ASTM C-39 [19] were used to test CS and static MOE, respectively, while ASTM C-78 [20] was used to evaluate three-point static flexural strength. Fig. 2 depicts the views of the instrumented falling weight impact machine setup before and after the impact. The machine contained a 2 kg hammer that could be dropped from heights ranging from 0.5 to 2 m; in the current studies, the hammer was released from a height of 0.5 m. During the test, the impact load history was monitored by means of a piezoelectric loadcell with a capacity of 100 kN positioned slightly above the impactor tup. 2 steel cylinders of 10 mm diameter, placed on adjustable right angled support, supported the samples. A sensitivity of 2 mV/g and accelerometer with a variety of 2500*g* (gravitational acceleration) was used to record the specimen accelerations during a collision near the edge at the midspan. The acceleration meter was fastened to the top of the prism near the edge at mid-span, while the drop hammer was in the middle. By means of a personal computer (PC) based data gathering system, findings from the accelerometer and loadcell were acquired at 0.2 s interval.

[21,22] gives the bending load(Pb) at the midspan of the prism:

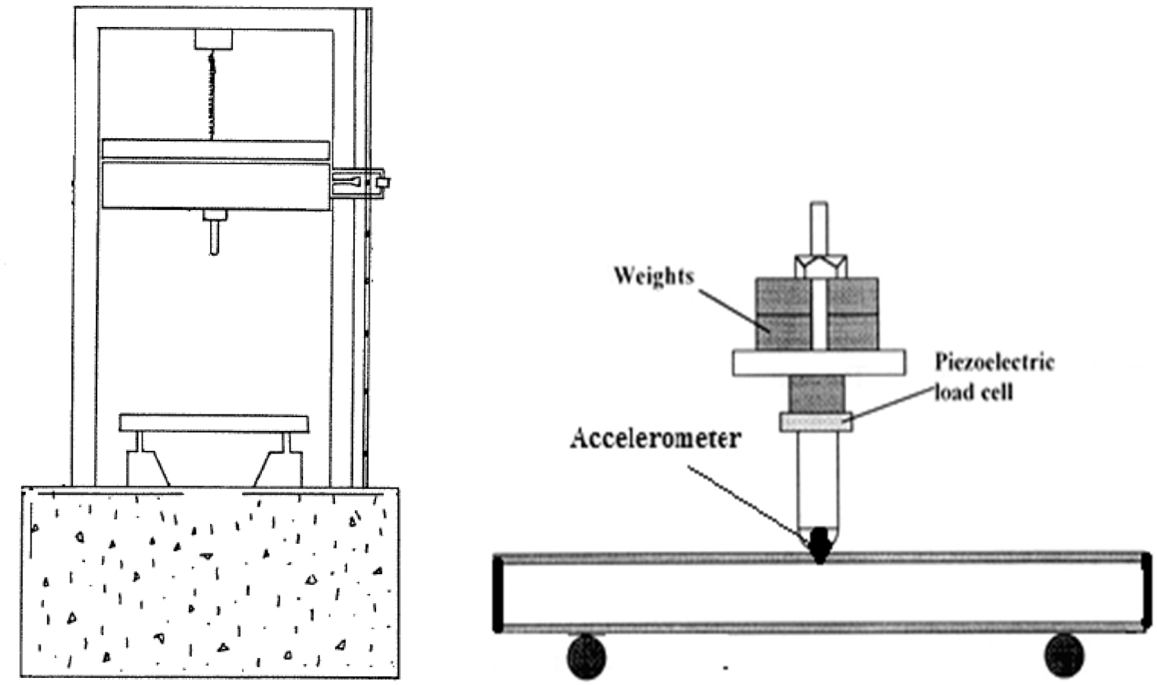

Fig. 2. The experimental flexural impact test rig.

$$P_b = P_t - P_i \quad (1)$$

For a linear distribution of accelerations, Pt is the tup (loadcell data) load and Pi(Eq. 2) is the initial load that is uniform along the prism.

$$P_i = \rho A a\,[L/3 + (8/3) \times (ov^3/L^2)] \quad (2)$$

where: "mass density of concrete; A cross sectional area of the prism; an acceleration at the center; L span of the test prism; and ov overhang length [21,22] provide the displacement history x (t) at the load" point:

$$x(t) = \int_0^t \int_0^t a(t)dt \quad (3)$$

a(t) denotes the acceleration as a function of time.

2.3. FEM

LUSAS was used to mimic the behavior of PW concrete prisms exposed to an I.L. The concrete prism was modeled by eight hexahedron corners (Fig. 3) by means of typical shape functions as shown in Eq. (4). Table 5 summarizes the associated shape functions

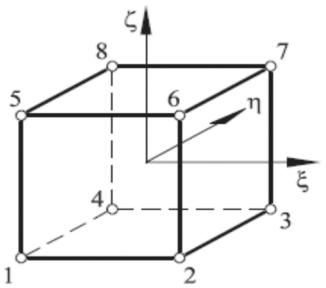

Fig. 3. The natural coordinates η, ξ, ζ and the eight-node hexahedron.

Table 5
The form functions for eigh-node hexahedrons.

$N_1^{(e)} = \frac{2}{16}(1-\eta)(1-\xi)(1-\zeta)$	$N_2^{(e)} = \frac{2}{16}(1-\eta)(1+\xi)(1-\mu)$	$N_3^{(e)} = \frac{2}{16}(1+\eta)(1+\xi)(1-\zeta)$
$N_4^{(e)} = \frac{2}{16}(1+\eta)(1-\xi)(1-\mu)$	$N_5^{(e)} = \frac{2}{16}(1-\eta)(1-\xi)(1+\zeta)$	$N_6^{(e)} = \frac{2}{16}(1-\eta)(1+\xi)(1+\mu)$
$N_7^{(e)} = \frac{2}{16}(1+\eta)(1+\xi)(1+\zeta)$	$N_8^{(e)} = \frac{2}{16}(1+\eta)(1-\xi)(1+\zeta)$	

for the hexahedron's eight nodes.

$$N_i^{(e)}(\xi,\eta,\zeta) = \frac{2}{16}(1+\xi_i\xi)(1+\zeta_i\zeta) \tag{4}$$

The following equation was used to determine the deformation:

$$\{u\} = \sum_{i=1}^{np}[N_i]\{u_i\} \tag{5}$$

where $\{u\}$: deformation vector anywhere above the member; $[N_i]$: Matrix of a complex nodal function with size(3×3); $\{u_i\}$: the deformation vector at the identified node of the member; *np*: the number of nodes in the member as a whole.

Boundary "terms (Fig. 4) were as follows: the prism was supported (distributed equally along the z-axis) from the bottom at x of 50 mm (support one) and x of 350 mm (support tow), and the tup load curve gotten from the experiment was utilized to describe the load at the location Pt (x = 200 mm, y = 50 mm, z = 50 mm). Several trials were conducted to govern the appropriate mesh size, and it was noticed that after 1024 member, there was no gain in precision; thus, this mesh size was" chosen.

The non linear dynamic equilibrium eq. [23,24] is as follows:

$$[M]\{a\} + [C]\{v\} + [K]\{d\} = \{f_e\} \tag{6}$$

where M represents the mass matrix defined as follows:

$$[M] = \sum_{e=1}^{n}\int_v [N]^{(e)T}\cdot[\rho]^{(e)}\cdot[N]^{(e)}dv \tag{7}$$

where N is the array of element shape functions and is the density matrix C denotes the Rayleigh damping matrix, which is given as:

$$[C] = a_R[M] + b_R[K] \tag{8}$$

where K denotes the structural stiffness matrix defined as follows:

$$[K] = \sum_{e=1}^{n}\int_v [B]^{(e)T}[D]^{(e)}[B]^{(e)}dv \tag{9}$$

where D is "the materials modulus matrix, and B is the strain displacement matrix; a_R (question 10) and b_R (question 11) are the Rayleigh damping coefficients of stiffness and" mass.

$$a_R = \frac{2\varpi_f\cdot\varpi_s(\psi_s\varpi_f - \psi_f\cdot\varpi_s)}{(\varpi_f^2 - \varpi_s^2)} \tag{10}$$

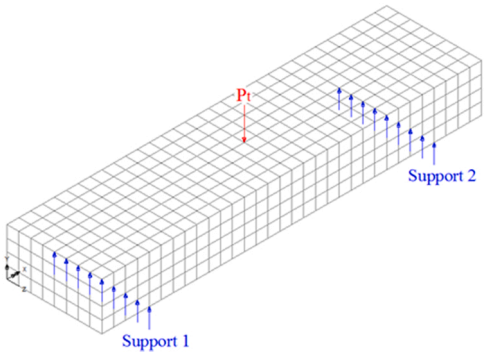

Fig. 4. FEM model for the prism.

$$b_R = \frac{2(\psi_f \varpi_f - \psi_s \varpi_s)}{(\varpi_f^2 - \varpi_s^2)} \tag{11}$$

where ψ_f and ψ_s are the damping ratio of the structure for first circular frequency(ϖ_f) and second circular frequency (ϖ_s) respectively [23]. The damping ratio for the first and second circular frequency is considered to be 5% [24]. The acceleration and hence the velocity and displacement increments for each time step were determined using an explicit (central difference) nonlinear dynamic approach. For issues requiring tiny time steps, like shock reaction from explosion or I.L, an explicit method is utilized [23].

The following is the central difference algorithm used in LUSAS [23]:

For each time step *n*.

$$\mathrm{M}a\ (t_n) = f\ (t_n) \tag{12}$$

$$v(\mathrm{t_{n+1/2}}) = v(\mathrm{t_{n-1/2}}) + \tfrac{1}{2}a(\mathrm{t_n})[\ \Delta \mathrm{t_n} - \Delta \mathrm{t_{n-1}}] \tag{13}$$

$$d\ (\mathrm{T_{n+1}}) = d\ (\mathrm{t_n}) + v\ (\mathrm{t}_{\ n+1/2})\ \Delta \mathrm{t_n} \tag{14}$$

where *a*, *v* and *d* are the acceleration, velocity, and displacement of any node.

LUSAS computes the time step for numerical stability.

3. Findings and discussion

3.1. Experimental findings

The compressive strength(CS) and MOE of several concrete mixtures with and without PW were determined. At the age of 28-d, specimens of 100 mm diameter, and 200 mm height cylinders were analyzed.

The average CS of concrete is seen in Fig. 5. When fine aggregate is replaced with PW, the average CS decreases by 26%, 38%, and 52%, with amounts, decreasing by 20%, 30%, and 40%, respectively. The MOE, as in Fig. 6 which decreases by 15%, 23%, and 34%, is similar. The decrease in CS and MOE caused by the addition of PW to the concrete as a fine aggregate substitute is also consistent with previous research by [13].

The lower CS of concrete is related to the plastic's mild CS in comparison to the compressive tension of natural fine aggregate. Furthermore, the poor bond between the cement pastes and the PW particle, as well as the deformability of the PW particle, results in the initiation of cracks around the PWs particle in a manner comparable to that which occurs in PW 0% concrete because of air voids, causes stress decrease.

Fig. 7 depicts the fluctuation of tup load with time, demonstrating that the total I.L rises with the addition of 20% and 30% PW particles as a fine aggregate substitution. Although the peak tup load for PW 40% is smaller than that of PW 30%, it is still more than that of PW 0% concrete. The increased overall I.L is related to plastic's greater plastic energy capacity when compared to regular concrete; hence, the inclusion of PW increases the mix's ductility and impact absorption capacity.

Fig. 8a-d depicts the time-dependent fluctuations in tup, inertial, and bending loads for PW concretes. The inertial load was determined using Eq. (2), and the bending load was derived by subtracting the inertial load from the tup load. Both inertial and bending loads rise for PW 20% and PW 30%, then drop for PW 40% but remain greater than for PW 0% concrete. Because PW enhances the flexibility of the composite mix, the inertial load rises. According to [25], increasing the PW enhances ductility and I.L absorption. [24] and [26] also determined that the lower the static bending strength, the greater the proportional increase in bending strength with increasing strain rate. These two factors work together to increase impact bending resistance. Increases in I.L, on the other hand, maybe because of the fact that under I.L, fractures are forced to propagate over short distances, which generally has PW with stronger damping and particles with higher strength than concrete.

Fig. 9 shows the computed impact bending load vs deflection graphs for PW 0%, PW 20%, PW 30%, and PW 40%. The fracture

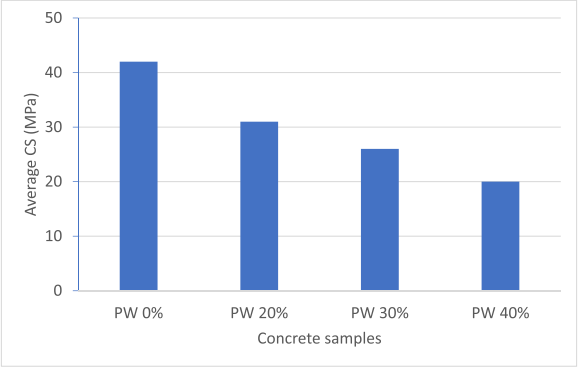

Fig. 5. Average CS against PW concrete.

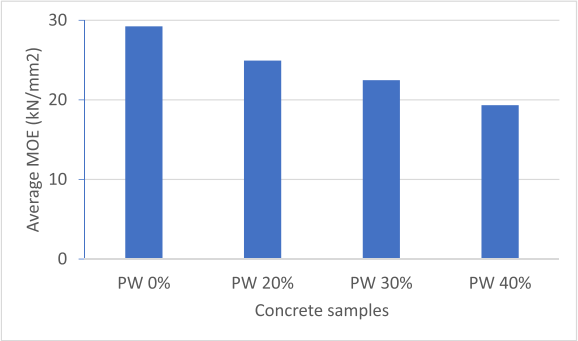

Fig. 6. Average MOE against PW concrete.

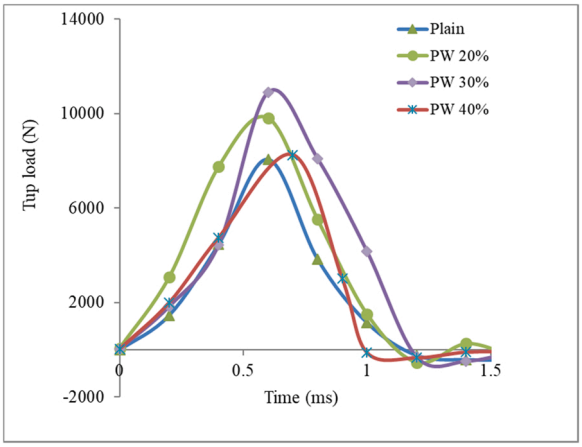

Fig. 7. Tup load history.

energies for the PW concrete samples are summarized in Table 4. The dynamic GF is greater than the static GF, as previously discovered [21,22,26] when normal concrete was utilized as the control mix. Under I.L, the GF of PW 0% is 1.41 Nm. The GF rises by 50% and 65% for PW by 20% and PW by 30%, respectively, whereas it only increases by 6% for PW by 40%.

Fig. 9 shows the computed impact bending load against deflection for PW 0% concrete and the three varieties of flexible concrete. The GF is described in this article as the area under the impact bending load against the displacement curve [21,22,26]. The GF for PW 0% and PW concretes are summarized in Table 4. As shown in refs. [21,22,26], dynamic GF is greater than static GF. Under I.L, the GF of PW 0% concrete is 1.41Nm. Under I.L, the concrete flexural energy with 5% and 10% PW is 190% and 240% more than that of PW 0% concrete under the same conditions, respectively, while a 67% increase is seen with 40% substitution.

3.2. Comparison of static and dynamic test results

Table 6 compares the findings of static bending (from the three-point static flexural loading test) tests to those of impact bending testing (from Eq. 1) and the GF is described in this article as the area under the impact bending load against the displacement curve [21, 22,26]. The static peak bending load is often smaller than the impact peak bending load, which is consistent with the published research [21,22,26]. It is also noted that as the proportion of PW rises, so does the ratio of dynamic to static peak bending loads. This is because of the fact that adding PW to concrete with a commensurate reduction in fine aggregate amount reduces its strength under static stress, yet the capacity of PW to absorb dynamic energy rises the concrete strength under I.L [27–30]. However, the ratio of dynamic to static GF rises only for PW 20 and PW 30%, and it drops but remains more than that of PW 0% for PW 40%.

3.3. Comparison of experimental and simulation results

Fig. 10 shows the actual data (Tup load from Fig. 7 and displacement from Eq. 3) compared to model data (Tup load from Fig. 7 and displacement from the 3D finite element technique), demonstrating the strength of the suggested model in dealing with the issue. When compared to regular concrete, the PW concrete samples have some minor differences that are tolerable. The displacement at the end of the impact reaction for PW 0% is 0.9 mm in simulation and 0.7 mm in an experiment. As the PW is added, the magnitudes of displacement rise somewhat for 20% and 30% PW additions and drop for 40% PW additions; this finding agrees well with the bending

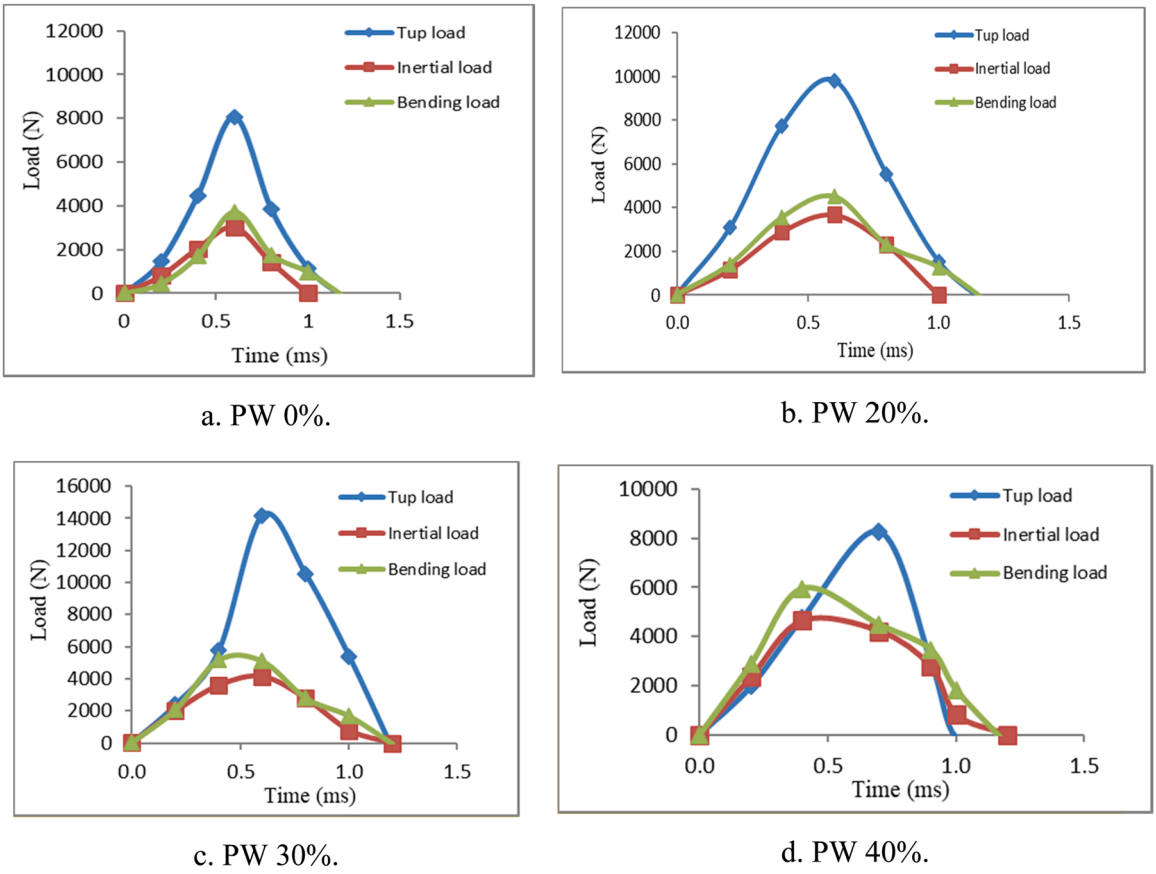

Fig. 8. Histories of Tup, inertial, and bending loads.

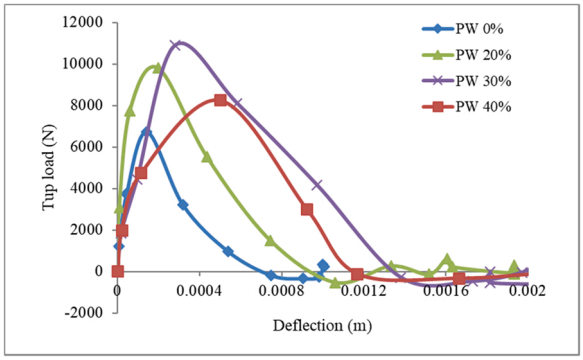

Fig. 9. Impact bending load vs. deflection.

Table 6
Experimental impact and static bending test findings comparison.

Concrete type	Impact results		Static results		Ratio: dynamic/static	
	Peak bending load	G_F	Peak bending load	G_F	Peak binding load	G_F
PW 0%	8075	1.42	4200	0.51	1.92	2.78
PW 20%	9809	4.12	2957	0.62	3.32	6.65
PW 30%	10,901	4.87	2766	0.64	3.94	7.61
PW 40%	8255	2.38	2598	0.58	3.18	4.10

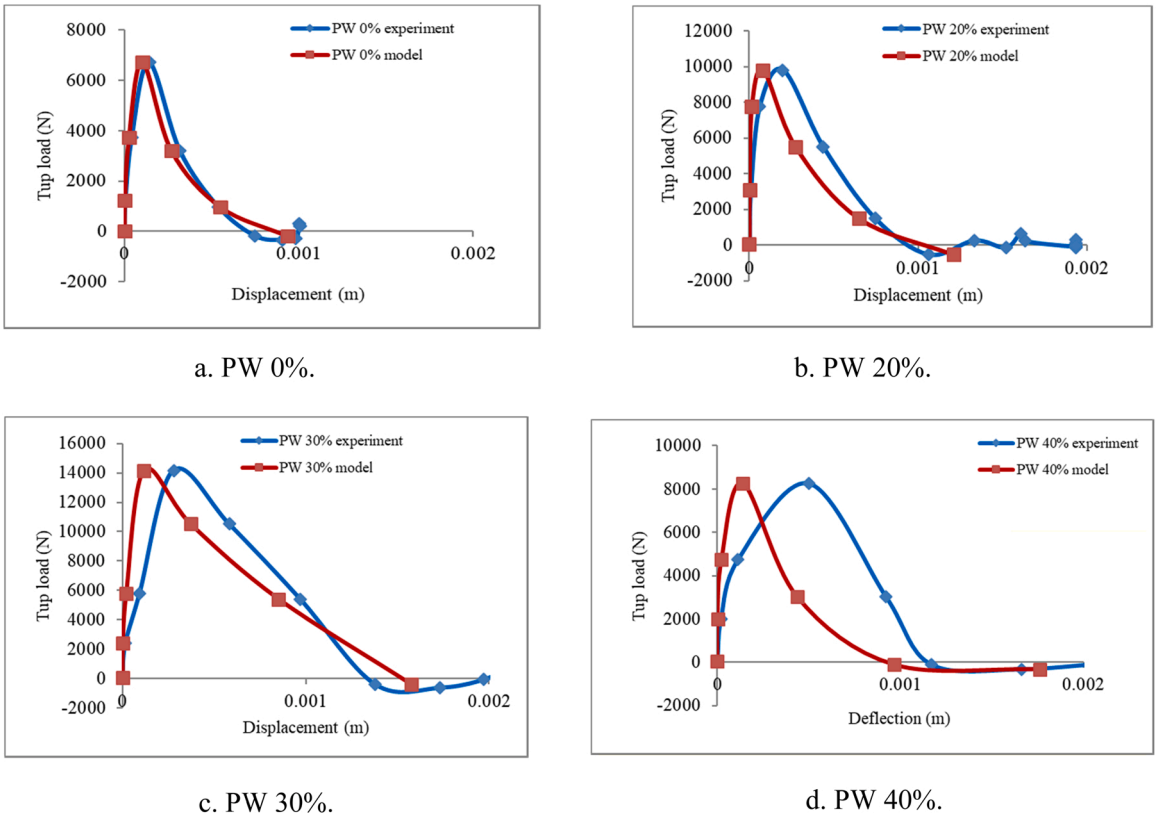

Fig. 10. I.L vs. displacement, experimental and projected.

load vs. displacement trend seen in Fig. 10.

4. Conclusion

The influence of substituting fine aggregate with PW on the I.L performance of concrete was examined. Concrete examples were made by adding 20%, 30%, and 40% PW to the mix and reducing the same percentage of fine aggregate. All samples were tested under impact and static stresses. The numerical predictions derived by the suggested FEM model were well aligned with the experimental data on impact L-D behavior. It was worth noting that the fine aggregate substitution by PW achieved increased the inertial load, impact tup, and bending load by up to 30%; at 40%, despite a minor decline, the findings were still better than PW's 0%. The static peak bending load consistently decreased as the PW amount increased, and the impact bending energies were always greater than the static energies. The suggested modeling technique would be a potential addition to facilitating accurate predictions of PW concretes, avoiding the need for time-consuming and dangerous experimental procedures.

Declaration of Competing Interest

The authors declare that they have no known competing financial interests or personal relationships that could have appeared to influence the work reported in this paper.

Data availability

The data that has been used is confidential.

References

[1] B.A. Tayeh, I. Almeshal, H.M. Magbool, H. Alabduljabbar, R. Alyousef, Performance of sustainable concrete containing different types of recycled plastic, J. Clean. Prod. 328 (2021), 129517.
[2] R. Siddique, J. Khatib, I. Kaur, Use of recycled plastic in concrete: a review, Waste Manag. 28 (10) (2008) 1835–1852.
[3] I. Almeshal, B.A. Tayeh, R. Alyousef, H. Alabduljabbar, A.M. Mohamed, A. Alaskar, Use of recycled plastic as fine aggregate in cementitious composites: a review, Constr. Build. Mater. 253 (2020), 119146.
[4] B. Bhardwaj, P. Kumar, Waste foundry sand in concrete: a review, Constr. Build. Mater. 156 (2017) 661–674.

[5] S. Yin, R. Tuladhar, F. Shi, M. Combe, T. Collister, N. Sivakugan, Use of macro plastic fibres in concrete: a review, Constr. Build. Mater. 93 (2015) 180–188.
[6] I. Almeshal, B.A. Tayeh, R. Alyousef, H. Alabduljabbar, A.M. Mohamed, Eco-friendly concrete containing recycled plastic as partial replacement for sand, J. Mater. Res. Technol. 9 (3) (2020) 4631–4643.
[7] S. Akçaözoğlu, C.D. Atiş, K. Akçaözoğlu, An investigation on the use of shredded waste PET bottles as aggregate in lightweight concrete, Waste Manag. 30 (2) (2010) 285–290.
[8] B.A. Tayeh, M.M. Al-Tayeb, I. Al-Daoor, S. Wafi, Ultimate Failure Resistance of Concrete with Partial Replacements of Sand by Polycarbonate Plastic Waste Under Impact Load, Civil and Environmental Research (2020).
[9] H. Mohammadhosseini, M.M. Tahir, A.R.M. Sam, N.H.A.S. Lim, M. Samadi, Enhanced performance for aggressive environments of green concrete composites reinforced with waste carpet fibers and palm oil fuel ash, J. Clean. Prod. 185 (2018) 252–265.
[10] H. Mohammadhosseini, A.A. Awal, J.B.M. Yatim, The impact resistance and mechanical properties of concrete reinforced with waste polypropylene carpet fibres, Constr. Build. Mater. 143 (2017) 147–157.
[11] H. Mohammadhosseini, M.M. Tahir, A.R.M. Sam, The feasibility of improving impact resistance and strength properties of sustainable concrete composites by adding waste metalized plastic fibres, Constr. Build. Mater. 169 (2018) 223–236.
[12] M.A.-T. Mustafa, I. Hanafi, R. Mahmoud, B. Tayeh, Effect of partial replacement of sand by plastic waste on impact resistance of concrete: experiment and simulation, Structures (2019) 519–526.
[13] Y.-W. Choi, D.-J. Moon, J.-S. Chung, S.-K. Cho, Effects of waste PET bottles aggregate on the properties of concrete, Cem. Concr. Res. 35 (4) (2005) 776–781.
[14] Z.Z. Ismail, E.A. Al-Hashmi, Use of waste plastic in concrete mixture as aggregate replacement, Waste Manag. 28 (11) (2008) 2041–2047.
[15] T.R. Naik, S.S. Singh, C.O. Huber, B.S. Brodersen, Use of post-consumer waste plastics in cement-based composites, Cem. Concr. Res. 26 (10) (1996) 1489–1492.
[16] A. Al-Manaseer, T. Dalal, Concrete containing plastic aggregates, Concr. Int. 19 (8) (1997) 47–52.
[17] A.I.C.C.-o. Concrete, C. Aggregates, Standard Practice for Making and Curing Concrete Test Specimens in the Laboratory, ASTM International, 2007.
[18] C. ASTM, Standard Test Method for Static Modulus of Elasticity and Poisson's Ratio of Concrete in Compression, Annual book of ASTM standards 4, 2002, p. 469.
[19] C. ASTM, Standard Test Method for Compressive Strength of Cylindrical Concrete Specimens, Chủ biên, 2012.
[20] C. ASTM, Standard Test Method for Flexural Strength of Concrete (Using Simple Beam with Third-point Loading), American society for testing and materials, 2010, 19428-2959.
[21] N. Banthia, S. Mindess, A. Bentur, M. Pigeon, Impact Testing of Concrete Using a Drop-weight Impact Machine, Exp. Mech. 29 (1) (1989) 63–69.
[22] N. Banthia, S. Mindess, A. Bentur, Impact behaviour of concrete beams, Mater. Struct. 20 (4) (1987) 293–302.
[23] A.K. Chopra, Dynamics of Structures, Pearson Education India, 2007.
[24] W. Suaris, S.P. Shah, Properties of concrete subjected to impact, J. Struct. Eng. 109 (7) (1983) 1727–1741.
[25] P. Asokan, M. Osmani, A.D. Price, Improvement of the mechanical properties of glass fibre reinforced plastic waste powder filled concrete, Constr. Build. Mater. 24 (4) (2010) 448–460.
[26] H. Fu, M. Erki, M. Seckin, Review of effects of loading rate on concrete in compression, J. Struct. Eng. 117 (12) (1991) 3645–3659.
[27] S.M.A. Qaidi, Y.Z. Dinkha, J.H. Haido, M.H. Ali, B.A. Tayeh, Engineering properties of sustainable green concrete incorporating eco-friendly aggregate of crumb rubber: a review, J. Clean. Prod. (2021), 129251.
[28] S.M.A. Qaidi, Y.S.S. Al-Kamaki, State-of-the-art review: concrete made of recycled waste PET as fine aggregate, J. Duhok Univ. 23 (2) (2021) 412–429.
[29] M.M.A.-T. Ibrahim Almeshal, Shaker M.A. Qaidi, B.H. Abu Bakar, Bassam A. Tayeh, Mechanical properties of eco-friendly cements-based glass powder in aggressive medium, Mater. Today Proc. 2214–7853 (2022).
[30] S.N. Ahmed, N.H. Sor, M.A. Ahmed, S.M.A. Qaidi, Thermal conductivity and hardened behavior of eco-friendly concrete incorporating waste polypropylene as fine aggregate, Mater. Today Proc, 2022.